Scanning Microscopy

Volume 1990
Number 4 *Fundamental Electron and Ion Beam Interactions with Solids for Microscopy, Microanalysis, and Microlithography*

Article 4

1990

Compton Scattering In Electron Energy Loss Spectrometry

P. Schattschneider
Technical University, Vienna, Austria, schattschnei@efh750.una.at

P. Pongratz
Technical University, Vienna, Austria

H. Hohenegger
Technical University, Vienna, Austria

Scanning Microscopy Supplement 4, 1990 (Pages 35-43)
Scanning Microscopy International, Chicago (AMF O'Hare), IL 60666 USA

0892-953X/90$3.00+.00

Compton Scattering in Electron Energy Loss Spectrometry

P. Schattschneider*, P. Pongratz and H. Hohenegger
Inst. f. Angewandte und Technische Physik, Techn. Univ. A-1040 Vienna, Austria

Abstract

It is well known that the distribution of electron momenta (electron density in momentum representation) of gases can be probed by Compton scattering of either photons (γ-rays or X-rays) or electrons. Recently it has been shown that Compton scattering of electrons is suited to the study of the electron momentum densities of solids on a microscopic scale. This technique, known as ECOSS, *Electron Compton Scattering from Solids* can be done in the electron microscope by electron energy loss spectrometry (EELS).

After a discussion of inherent approximations and the introduction of the reciprocal form factor a method is proposed in order to cope with the main difficulty, namely multiple scattering. Important applications of ECOSS are the study of anisotropy of momentum densities; correlation effects of conduction electrons in metals; and charge transfer in alloys.

Keywords: electron Compton scattering, electron momentum density, reciprocal form factor, multiple scattering, anisotropy, electron correlation.

*Address for Correspondence:
P. Schattschneider
Institut für Angewandte und Technische Physik,
Techn. Universität Wien.
Wiedner Hauptstr. 8-10, A-1040 Vienna, Austria
Phone: (222) 58801-5626
Fax: (222) 56 42 03
Bitnet: Schattschnei@efh750.una.at

Introduction

Electron energy loss spectrometry (EELS) in the electron microscope is well suited to the study of the electron momentum densities of solids on a microscopic scale. This technique is known as ECOSS, *Electron Compton Scattering from Solids*. [10, 11].

Like in the photon case, the energy of the scattered electron is increasingly lowered with scattering angle; the energy distribution has a halfwidth proportional to the mean squared momentum of the scatterer (*Doppler broadening*). The shape of the distribution can be shown to be an image of the momentum distribution of the electron in the ground state.

Technically, ECOSS is EELS in diffraction mode at high scattering angles ($\sim 100\,mrad$) in the energy range of the maximum of the Bethe surface. Since the cross section for scattering of electrons is some five orders of magnitude larger than that of photons, and since the intensity of electron sources is $\sim 10^2$ larger than for typical photon sources, it is evident that the sensitivity of ECOSS enormously exceeds that of photon Compton scattering, or the duration of an experiment can be reduced from days (for photon scattering) to hours or minutes.

Another fact worth noting is that, contrary to the photon case, a very high spatial resolution can be achieved as in conventional TEMs, which is important for the investigation of anisotropy in fine crystalline material.

ECOSS is a relatively new technique. Radiation damage of the specimen and multiple scattering restricted application mainly to gaseous specimens. Only in 1981, the first ECOSS experiment was reported [10]. Later on, the electron momentum distribution in graphite was measured [9]. See later (Applications). Almost all of the few experimental and theoretical works performed so far concentrate on optimization of measurement conditions and comparison with photon Compton scattering [10, 11, 8]. The theory is well understood by now, and modern spectrometers, especially with parallel detection, in combination with high brightness electron sources, are suited for application of this technique.

Theory

Starting with first order perturbation theory we get

Symbol table

a_p	momentum state annihilation operator
a_p^+	momentum state creation operator
B	reciprocal form factor
E	energy, energy loss
F	static form factor
H	Hamiltonian of perturbed system
H_0	Hamiltonian of unperturbed system
$\hbar$	Plancks constant $/2\pi$
J	Compton profile
$k_{a(b)}$	wave numbers of incident (scattered) electron
m	electron mass
$n(r)$	particle density operator
p, q	momentum vectors
p_F	Fermi momentum
r	space coordinates
$S(q,\omega)$	dynamic form factor
t	time (parameter)
V	perturbation potential
$\|\varphi>$	ground state Hilbert space vector
ψ, ψ^+	field operators
$\chi(\vec{p})$	ground state momentum space wave function
ρ_q	density operator in momentum representation
σ	scattering cross section
θ	scattering angle
Ω	solid angle
ω	frequency

Throughout the paper, the Dirac notation is used. Formulae and expressions are in SI-units unless otherwise specified.

---

for the dynamical form factor:

$$S(q,\omega) := \frac{1}{2\pi\hbar}\int_{-\infty}^{+\infty} e^{-i\omega t} < \varphi|e^{iHt/\hbar}\rho_q e^{-iHt/\hbar}\rho_{-q}|\varphi > dt. \tag{1}$$

ω relates to the energy E lost by the scattered electron as $E = \hbar\omega$, H the Hamiltonian of the perturbed system, ρ_q is the density operator, and $|\varphi>$ the ground state wave function of the scatterer. The Hamiltonian consists of an unperturbed part H_0 and a perturbation V

$$H = H_0 + V. \tag{2}$$

Here H_0 is the kinetic energy operator and V the potential of the binding forces. The exponential can be expanded in a power series [5]

$$e^{iHt} = e^{iH_0 t}\cdot e^{iVt}\cdot e^{-[H_0,V]t^2/2}\ldots \tag{3}$$

For high energy transfer, the time integration contributes during a short interaction time $t \sim \omega^{-1}$ only, and one can set

$$exp\left(-\frac{1}{2}[H_0,V]t^2\right) \approx 1. \tag{4}$$

The higher terms contain multiple commutators and are of higher order in time. The potential $V(\vec{r})$ can be commuted with $\rho_q = e^{iqr}$, so it vanishes in the matrix element. To put it physically, the potential in which the electron moves can be considered constant for the short time of interaction and eq. 1 becomes

$$S = \frac{1}{2\pi\hbar}\int_{-\infty}^{+\infty} e^{-i\omega t} < \varphi|e^{iH_0 t/\hbar}\rho_q e^{-iH_0 t/\hbar}\rho_{-q}|\varphi > dt. \tag{5}$$

By use of the time dependent Heisenberg operator

$$\rho_q(t) = e^{iH_0 t/\hbar}\rho_q e^{-iH_0 t/\hbar} \tag{6}$$

this is

$$S = \frac{1}{2\pi\hbar}\int_{-\infty}^{+\infty} e^{-i\omega t} < \varphi|\rho_q(t)\rho_{-q}(0)|\varphi > dt. \tag{7}$$

The momentum density operator $\rho_q(t)$ is the Fourier transform of the ordinary density operator $n(r)$

$$n(r) = \psi(r)\psi^+(r) \tag{8}$$

where $\psi(r)$ are field operators. From the Wiener-Khintchin theorem, we know that the Fourier transform of the product in eq. (8) is the autocorrelation of the field operators in momentum representation, so

$$< \rho_q(t)\rho_q^+(0) >= \sum_{p,p'} < a_p^+(t)a_{p+q}(t)a_{p'+q}^+ a_{p'} > \tag{9}$$

where the sum is over p-states within the Fermi sphere. a^+, a are creation and annihilation operators. For large momentum transfer q, which is assumed henceforth, the final state electron can be considered to be free. For free electrons, $a_p^+(t) = a_p^+(0)exp(-ip^2/2m)t$, and we may write

$$< \rho_q(t)\rho_q^+(0) >= \sum_{p,p'} < a_p^+ a_{p+q}a_{p'+q}^+ a_{p'} > \cdot e^{(-ip^2/2m)t}e^{i(p+q)^2/2m)t} \tag{10}$$

The second aspect of large momentum transfer is that the operator $a_{p'+q}^+$ creates a particle in the previously empty state $p'+q$ far beyond the Fermi momentum. Subsequent annihilation of a particle in state $p+q$ is only possible when there *is* a particle, i. e. only for $p = p'$ otherwise the probability amplitude for this process vanishes. See Fig. 1b. Hence

$$a_{p+q}a_{p'+q}^+ = \begin{cases} 0 & p \neq p' \\ 1 - n_{p+q} = 1 & p = p'. \end{cases} \tag{11}$$

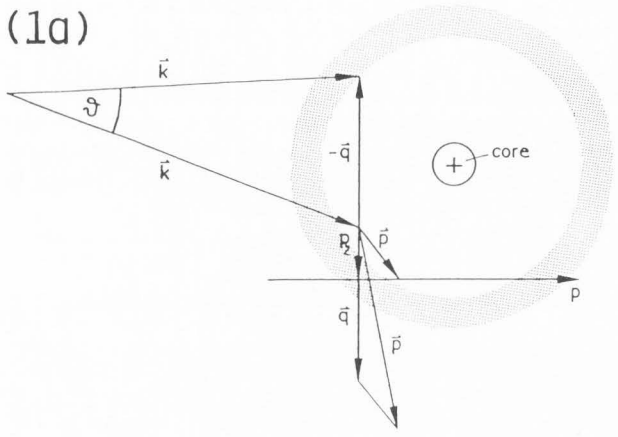

Fig. 1a: Geometry of Compton scattering. $\vec{p}$ is the initial wave vector of the target electron, $\hbar\vec{q}$ is the momentum transferred in the interaction, $\vec{p}_f$ is the final wave vector of the target electron. The quantity measured in Compton scattering is the distribution of initial wave vectors $\vec{p}$ projected onto the $\vec{q}$ direction, p_z. The dotted area schematically indicates the spatial distribution of valence electrons.

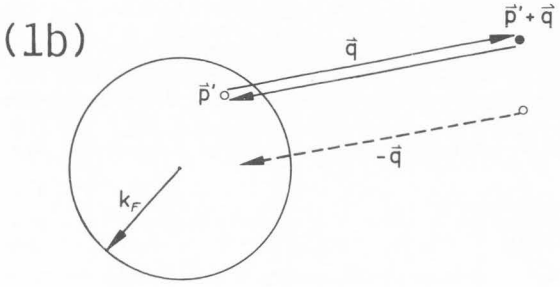

Fig. 1b: Sketch of the Fermi sphere with allowed creation and annihilation processes (full lines). The process indicated by a dashed line is forbidden.

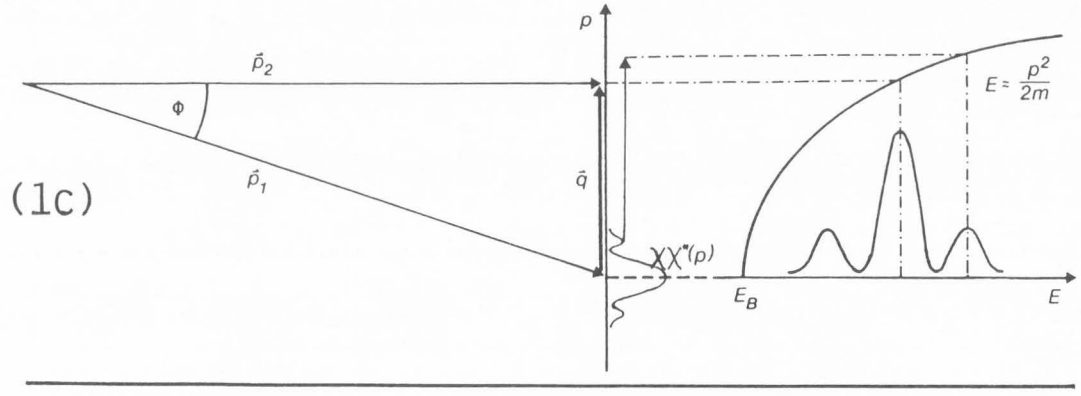

Fig. 1c: Scattering geometry and relationship between ground state momentum density $\chi\chi^*$ and Compton profile. The latter is a projection of the former onto the energy loss E via the free electron parabola.

Eventually,

$$< \rho_q(t)\rho_q^+(0) >= \sum_p < a_p^+ a_p > e^{i((p+q)^2-p^2)/2m)t} \quad (12)$$

Replacing the sum in eq. (12) by an integral $\left(\sum_p \to \int \frac{d^3p}{(2\pi)^3}\right)$ and the time integral in eq. (5) by an appropriate δ-function yields

$$S = \int \frac{d^3p}{(2\pi)^3} \delta\left(E - \frac{q^2}{2m} - \frac{\vec{q}\vec{p}}{m}\right) \cdot \rho(\vec{p}) \quad (13)$$

where we have introduced the momentum distribution

$$\rho(\vec{p}) = \chi(\vec{p})\chi^*(\vec{p}) =< a_p^+ a_p > . \quad (14)$$

The one-partice momentum distribution in the many-particle system is defined as

$$\begin{aligned} \rho(\vec{p}_1) &= \int d^3p_2 ... d^3p_n \chi(\vec{p}_1, ...\vec{p}_n)\chi^*(\vec{p}1, ...\vec{p}_n) \\ &= \chi(\vec{p}_1)\chi^*(\vec{p}_1). \end{aligned} \quad (15)$$

$\chi(\vec{p})$ is the one electron wave function of the ground state in momentum representation. It should be noticed here that the last equality does not strictly hold in an interacting n-particle system where a one-electron wave function does not exist. Rather, one should use a density matrix formulation. Though, we identify $\rho(\vec{p})$ with the square of a one-electron wave function henceforth.

In the last step of the derivation, we integrate the δ-function and use the relationship [10] between S and the differential cross section $\partial^2\sigma/\partial E\partial\Omega$,

$$\frac{\partial^2\sigma}{\partial E\partial\Omega} = \left[\frac{2me^2}{(\hbar q)^2}\right]^2 \frac{k_b}{k_a}\int \frac{d^2p_{xy}}{(2\pi)^2}\frac{m}{q}\cdot\rho(p_{xy},p_z), \qquad p_z = \frac{Em}{q} - \frac{q}{2} \tag{16}$$

Here, k_a k_b are the electron wave numbers of the incident and scattered electron respectively, E is the energy loss, and $\vec{q}$ is the momentum transfer. The variable p_z is the momentum component in the direction of $\vec{q}$. The scattering angle Ω relates to the quantities on the right by the scattering geometry (Fig. 1c).

The quantity $J(p_z)$ in eq. (16), called Compton profile

$$J(p_z) = \int d^2p_{xy}\rho(p_{xy},p_z) \tag{17}$$

can be derived directly from experiment. It is a projection of the 3-dimensional momentum density of the scatterer onto the direction of the scattering vector $\vec{q}$. It is, in principle, possible to obtain the complete 3-dimensional distribution $\rho(\vec{p})$ from a series of Compton experiments [6].

For fast probe electrons, then, and when the energy and momentum transfer in the interaction is large, the target electrons in the ground state can be treated *as if they were free, but having a momentum distribution as if they were bound.* This is the essence of the impulse approximation (IA), valid for large energy and momentum transfer in the Compton event.

The reciprocal form factor

Compton scattering provides information on the momentum density of electrons in the specimen. However, the same is true for elastic scattering which yields the modulus of the static form factor (the Fourier transform of the particle density):

$$F(\vec{p}) = \int d^3r\rho(\vec{r})e^{i\vec{p}\vec{r}}. \tag{18}$$

Taken for granted that the phase problem can be solved (determination of the phase of F) the question is legitimate whether $F(\vec{p})$ and $\rho(\vec{p})$ contain different physical information.

Eq. (18) says that F is the Fourier transform of ρ. Identifying ρ with the particle density in terms of one-electron wave functions,

$$\rho(\vec{r}) = \varphi(\vec{r})\varphi^*(\vec{r}), \tag{19}$$

(see the comment given after eq. 15) , we can apply the Wiener-Khintchin theorem stating that F is the autocorrelation function of the wave function χ in momentum representation

$$F(\vec{p}) = \int d^3p'\chi(\vec{p}+\vec{p'})\chi^*(\vec{p'}). \tag{20}$$

On the other hand, the quantity derived from Compton scattering is

$$\rho(\vec{p}) = \chi(\vec{p})\chi^*(\vec{p}) =< a_p^+ a_p > \tag{21}$$

i.e. the diagonal element of the density matrix in momentum representation. F and ρ contain cemplementary information. The latter is the probability of finding an electron with momentum $\vec{p}$, and doesn't give any clue to the phase of χ. The static structure factor F on the other hand contains information on the phases of wave functions, via the autocorrelation integral, but χ cannot be derived uniquely from F.

The Fourier transforms of eqs. (20) and (21) are

$$\rho(\vec{r}) = \int d^3pF(\vec{p})e^{-i\vec{p}\vec{r}} = \varphi(\vec{r})\varphi^*(\vec{r}) =< \psi^+(\vec{r})\psi(\vec{r}) >, \tag{22}$$

$$B(\vec{r}) = \int d^3p\rho(\vec{p})e^{-i\vec{p}\vec{r}} = \int d^3r'\varphi(\vec{r}+\vec{r'})\varphi^*(\vec{r'}). \tag{23}$$

Note the formal symmetry of eqs. (21, 22) and eqs. (20, 23).

B is called reciprocal form factor because of its similarity to F. In complete analogy to the statement on the momentum space quantities F, ρ it can be said that elastic scattering yields the diagonal element of the density matrix in real space (probability of finding an electron at position $\vec{r}$) without any clue to the phases of wave functions. Compton scattering yields, via the reciprocal form factor B, information on the phase relations of the wave function φ at different $\vec{r}$.

The different information contents of F and J are illustrated in the following highly schematic example: A free electron with wave function

$$\varphi(\vec{r}) = e^{i\vec{k}\vec{r}} \tag{24}$$

has constant charge density

$$\rho = \varphi\varphi^* = 1 \tag{25a}$$

over the entire space (normalization factors are neglected here). Elastic scattering yields a delta-function for the static structure factor F

$$F(\vec{p}) \propto \int d^3r\rho(\vec{r})e^{i\vec{p}\vec{r}} = \delta(\vec{p}) \tag{25b}$$

consistent with the constant charge density. There is no way to tell the wave vector of the scatterer since the phase cancels in the density.

The CP of the moving electron is likewise a delta function, at $p_z = k$, corresponding to an energy

$$E = \frac{kq}{m} + \frac{q^2}{2m} \tag{26}$$

when the scattering vector $\vec{q}$ is parallel to $\vec{k}$. The momentum density follows from eqs. (16, 17)

$$\rho(\vec{p}) \propto \delta(\vec{p}+\vec{k}). \tag{27}$$

The reciprocal form factor B is, according to eq. (23),

$$B(\vec{r}) \propto e^{i\vec{k}\vec{r}}. \tag{28}$$

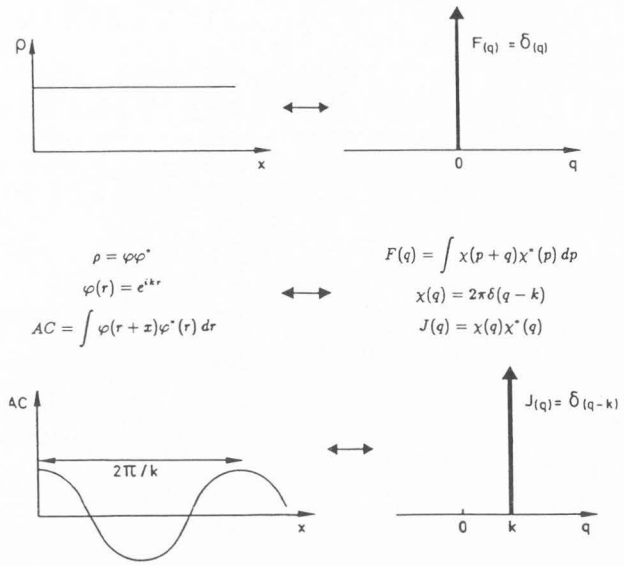

Fig. 2: Complementary information obtained from elastic scattering (top) and Compton scattering (bottom) for the highly schematic example of a plane wave: From the experimentally accessible static structure factor $F(q) = \delta(q)$ the charge density $\rho(x) = const.$ can be derived, but no information on the phase of the wave function is available. From the Compton profile $J(q)$, the reciprocal structure factor $B(x)$ can be derived, which is the autocorrelation function (AC) of the wave function. AC contains phase information from which the wave vector k of the plane wave can be derived.

Oscillations in B are caused by the r–dependent phase of ϕ. Since B is the autocorrelation of the wave function φ it is immediately obvious that the phase of the wave changes by 2π over the periodicity interval of B which is $2\pi/k$, See Fig. 2. So we have gained important information on the phase of the wave function which was not possible from elastic scattering data.

Contributions to the Compton Profile

Core electrons

The simple relationship between the momentum density and the differential cross section does no longer hold when the impulse approximation breaks down . One has to use a more accurate wave function for the final state in the matrix element. The exact hydrogenic (EH) approximation takes both φ_i and φ_f as screened hydrogenic atomic wave functions. Results of those calculations were published by Eisenberger and Platzmann [5] for K-shell electrons and by Bloch and Mendelsohn [3] for L-shell electrons. Hydrogenic models ignore electron exchange and correlation, but deliver analytical expressions for the generalized oscillator strenght (GOS), and give reasonable cross sections which appear to be in good agreement with the available experimental data [4]. The importance of the use of a more accurate model for the core electrons lies in the fact that an accurate core subtraction is necessary to get the pure valence electron CP which is of primary interest in most cases.

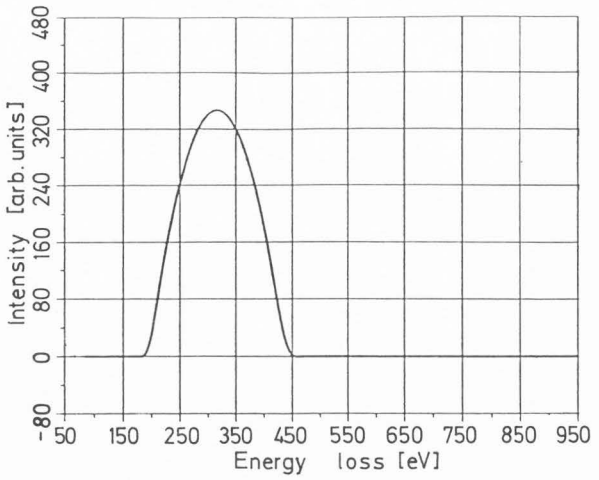

Fig. 3: Single scattering profile for conduction electrons (Al, 5.2 deg).

Conduction electrons

For the conduction electrons the simple free electron model can often be used. In the following example, this model was applied to polycristalline aluminum. From eq. (17) we get for the CP, by projecting the states within the Fermi sphere onto the direction p_z, the characteristic free electron parabola falling to zero at the Fermi momentum $\pm p_F$. See Fig. 3. In contrast to the L-electrons, the IA is valid for conduction electrons.

Multiple scattering

Aside from the Compton effect, other electronic excitations within the solid must be considered. Low-angle scattering off valence electrons gives rise to plasmon excitations peaking in the low energy loss region. Such a plasmon event can be followed by a Compton event. An equally dominant contribution to multiple scattering in the energy and momentum range of typical Compton experiments arises from Bragg- Compton double-scattering events. The Bragg rings and plasmon peaks can be considered as new sources for Compton events. In the typical range of Compton scattering, multiple scattering is caused by elastic scattering into high angles followed by a Compton event. Since these Compton events correspond to scattering angles different from the single Compton scattering angle new Compton profiles are generated with different maxima and width. They overlap with the single Compton profile and alter the position of the maximum and its width. To determine the Bragg scattering intensity, a radial density distribution in the diffraction pattern can be used. The intensities of successive plasmon events are found by integrating plasmon spectra in the bright field mode. The same result can be derived from the fact that, assuming independent scattering events, the intensities of succesive plasmon excitations obey Poisson statistics. These two mechanisms give rise to multiple scattering up to 50% and more of the Compton peak value. The

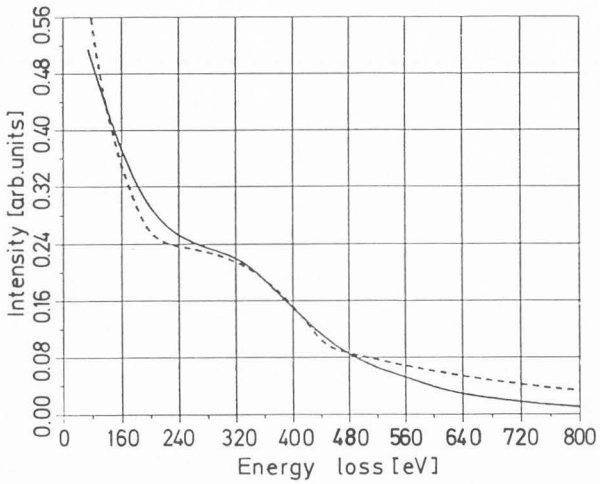

Fig. 4: Measured profile as compared with least squares fit over entire energy range (dashed). ($24nm$ Al, 5.2 deg).

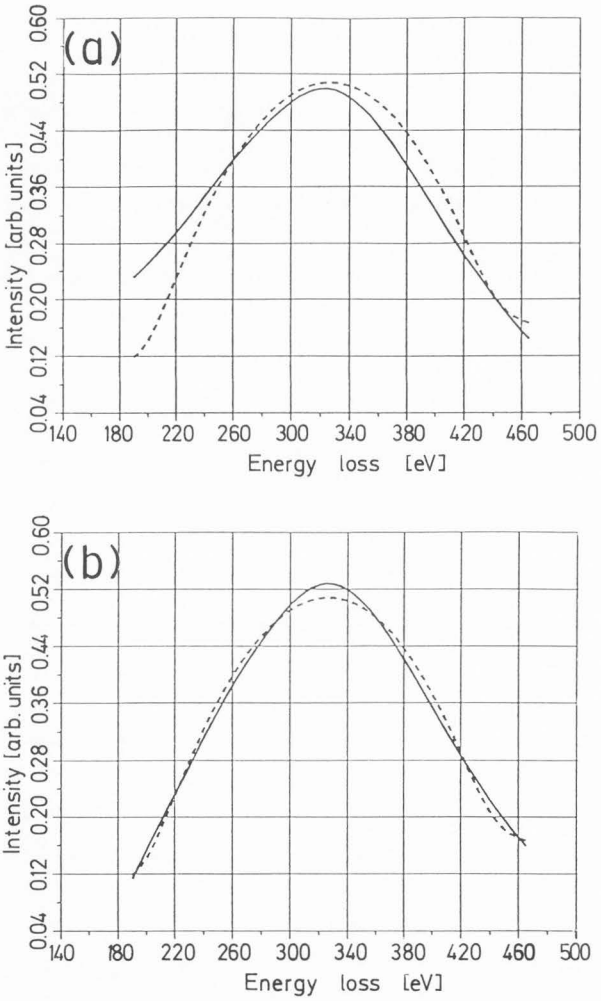

Fig. 5: Least squares fit excluding background as compared with prediction of scattering theory (dashed) for $24nm$ Al at $5.2deg$. Fitting region $115eV - 650eV$ (a), $190eV - 470eV$ (b).

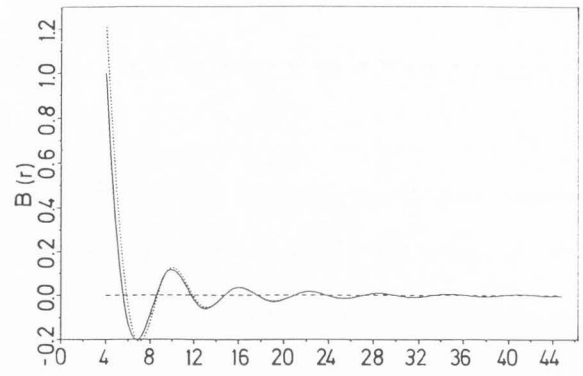

Fig. 6: Reciprocal form factor $B(r)$ of measured Compton profile including and excluding (dotted) L-shell contribution.

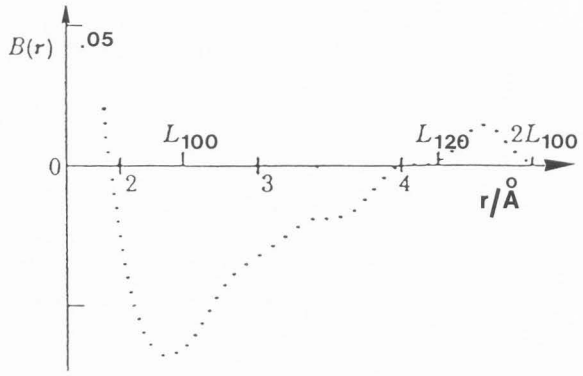

Fig. 7: Reciprocal form factor in $< 100 >$ direction in the basal plane of graphite, derived from ECOSS. Lattice points are denoted L_{ijk}. From [9].

measured spectrum may look completely erratic as was shown by a numerical simulation of CPs by Williams *et al* [12].

The angular dependence of the ratio of Compton peak intensity to multiple scattering contributions is very weak, hence using a higher scattering angle does not improve this ratio but rather decreases the intensity of the scattered electrons in accord with the $\sin\theta^{-4}$ behaviour (cf.eq. (16)).

When there is a continuum of scattering angles for the coupling of Bragg and Compton events—as is the case in polycrystalline specimens with well defined Bragg rings—the double scattering contribution forms a smoothly decreasing background dominated by the ionisation event with the smallest scattering angle. This is why the background approximately follows a power law dependence in energy ($A \cdot E^{-s}$), well known from inner-shell losses. Additional quasielastic processes play a minor role in shaping the background.

The coefficient A takes on a wide range of values, but s is generally in the range 2-6 [11]. Increasing specimen thickness lowers the value of s due to plural scattering contributions, and increasing energy loss increases this value.

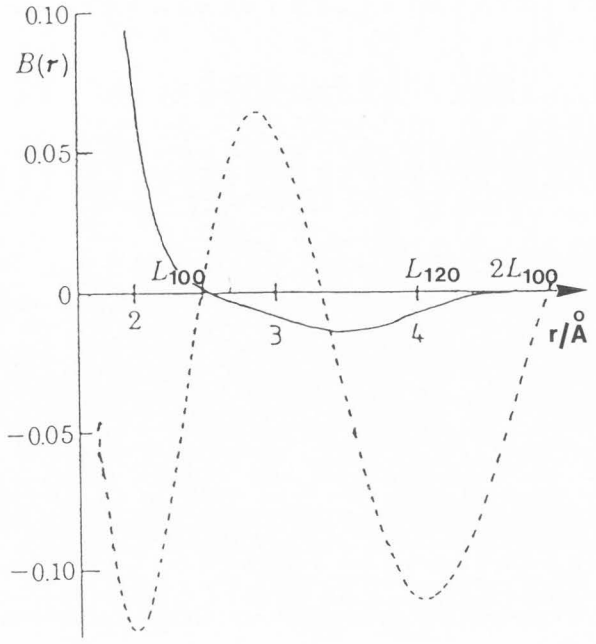

Fig. 8: Calculated reciprocal form factors averaged in the basal plane of graphite. Full line: Tight binding, dashed line: pseudopotential. From [9].

Due to this dependence of the coefficients A and s, they should be determined at each ionization edge. Usually the energy dependence of the background is measured over a fitting region immediately preceding the edge. This procedure can be considered valid if the coefficients remain constant over a certain range of interest beyond the ionization threshold. This method becomes problematic if the ionization threshold cannot be identified exactly as a result of multiple scattering contributions. In addition the increasing broadening of the spectra requires fitting within regions too wide for the coefficients in the power law dependence of the background to be considered constant. This gives rise to uncertainties in background subtraction, since, especially with the signal-noise ratio encountered in ECOSS experiments, which is worse than with the γ-ray technique, the Compton profile is rather sensitive to the background subtraction. One method, although not rigorous, to investigate the background behaviour is to fit a model calculation of the Compton profile, including multiple scattering contributions and a power law background, to the measured profile. This was done in the following demonstration experiment on aluminum.

Applications

Polycrystalline aluminum

In a demonstration experiment [8] CPs of polycrystalline aluminum were taken at a scattering angle of 5.2 degrees. Measurements were done on a cylindrical mirror analyzer (CMA) attached to a Siemens Elmiskop IA at $40keV$.The angular resolution was $\pm 2.4mrad$, corresponding to a wavenumber resolution of ± 0.25 Å^{-1}. The finite wavenumber resolution broadens the profiles by $\pm 15eV$ which amounts to a momentum uncertainty of $0.23a.u.$ This is considerably better than accuracies obtained from photon CS experiments ($\sim 0.4\,a.u.$ typically). The film thickness was 240 Å.

Measured CPs were fitted to calculations including L-shell- and conduction electrons as well as a background $\sim AE^{-s}$. From figs. 4, 5 it can be seen that the quality of the fitting depends on the fitting range. If the region of valence electron contribution is chosen, a deviation of $3\% - 4\%$ is found. In cases of a wider energy loss range for the fitting procedure the deviations increase up to almost 100%. These results clearly show that background subtraction (i.e. choice of an appropriate fitting region) is a serious problem.

From our calculations it is clear that, although the IA is valid for the conduction electrons, it is not for L-shell electrons. The maximum of the L-shell CP is $\sim 50eV$ higher than predicted by the IA. This effect causes the maximum of the measured profile - which is in essence a superposition of both contributions - to lie between the IA and the exact maximum. Consequently, it does not make much sense to interpret the total CP as the electron momentum density.

The asymmetry of the profile brings a commonly used practice in CP data processing into question, *viz.* to split the measured profile at its maximum and substitute the low energy part by the symmetrically extended high energy part. The reasoning is that multiple scattering contributes mainly in the low energy region of the profile. Given the experimental conditions encountered in ECOSS this procedure is not generally valid, both because the asymmetry caused by the core contributions is not taken into account, and because multiple scattering is not negligible even in the high energy part of the spectra. In practical applications the situation is rather better, since multiple scattering and core contributions— both flat and broad distributions— don't much influence the widely used reciprocal form factor $B(r)$.

It is evident from Fig. 6 that the L-shell contribution alters $B(r)$ only at small wave number.

Anisotropy in graphite

In an electron Compton scattering study of graphite, Vasudevan *et al.* [9] found strong anisotropy of the momentum distribution within the basal plane.(Fig. 7). Photon CS cannot give these results because the beam cannot be focused onto a single platelet of graphite the orientation of which is random in the basal plane. For comparison, Fig. 8 shows predictions of various theories. The disagreement is striking. The authors speculate that antibonding $sp_2\,\pi^*$ orbitals—which should be empty theoretically—may cause the large negative value of B at the lattice vector L_{100}. One fact is obvious: Even todays most refined model calculations are too poor for the prediction of CS data. This may well be since these calculations have, in general, not been used to predict wave functions but energy levels and band structure rather. In any case, one should be cautious about the results of these first ECOSS experiments.

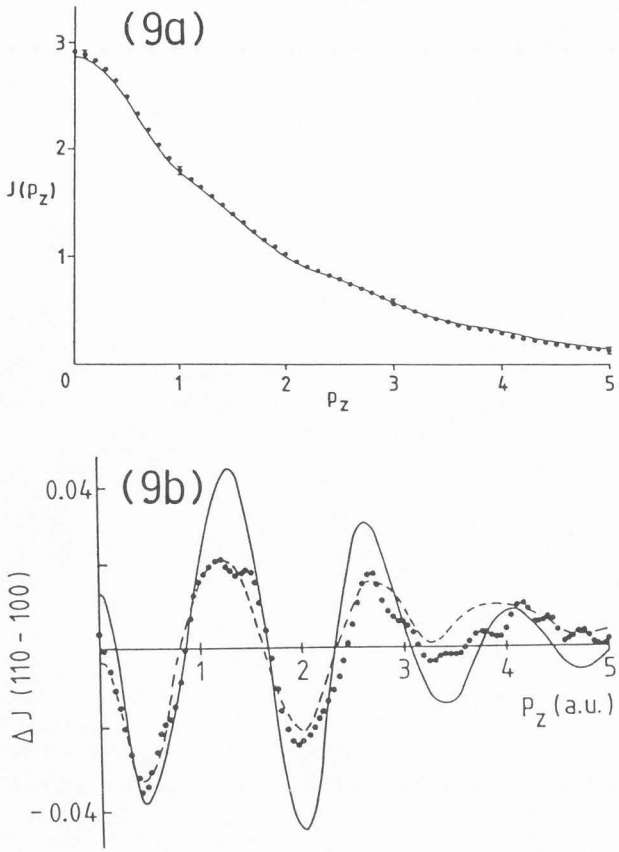

Fig. 9a: Compton profile for the valence electrons of Cu. Dots: experiment; full line: theory. From [7].
Fig. 9b: Experimental anisotropy in the Compton profile of Cu in directions $< 110 > - < 100 >$. Dotted and dashed lines: experiment; full line: theory (SCF-LDA) in the Hohenberg-Kohn-Sham formalism. From [7].

Electron correlation in copper

In order to demonstrate what can be expected for future ECOSS experiments we quote some results from photon Compton scattering: Fig. 9.a shows a Compton profile of the valence electrons in Cu, along the $< 110 >$ direction [7]. The theory which is an SCF local density approximation (LDA) with exchange/correlation correction using linearly combined Gaussian orbitals predicts the experiment quite well. However, when the anisotropy of the profile is plotted, the situation is different: Fig. 9.b shows that theory overestimates the amplitude of oscillations. In later papers [1, 2] the local density approximation was re-investigated thoroughly. The periodic deviations of LDA predictions from measurement, given in Fig. 10 were traced back to electron correlation effects in the inhomogeneous electron gas as the most probable reason. They act so as to reduce the occupation of the Fermi sphere relative to any model calculation based on a single particle concept. In an extended zone scheme, this effect gives rise to the oscillations in Fig. 10. Again it can be said that present theories of the electronic structure in the solid are too poor to predict Compton profiles accurately.

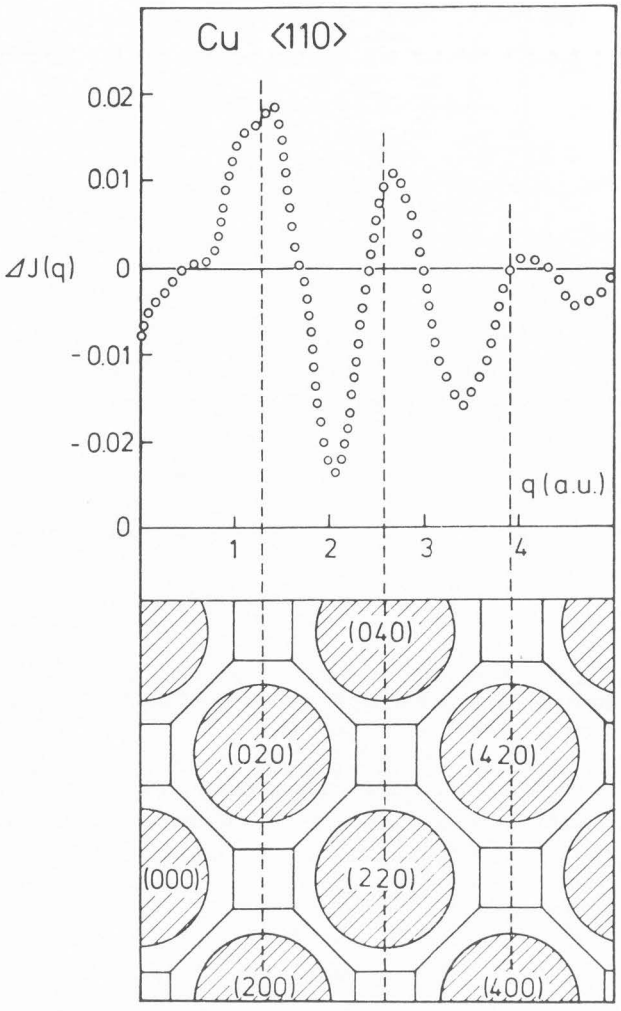

Fig. 10: Difference in the Compton profile betweeen SCF-LDA theory and experiment. In the lower part, a projection of the reciprocal lattice onto the $< 100 >, < 010 >$ plane with the Fermi surface of Cu is depicted. The oscillatory difference can be explained by the removal of states within the Fermi body to outside. From [2].

Conclusion

After a presentation of the theory of electron Compton scattering, the advantages and disadvantages with respect to established photon Compton scattering experiments are discussed. Examples show that a) the main obstacle of strong multiple scattering can be overcome by a careful analysis of the various contributions to the Compton profile; b) anisotropies in the momentum distribution of valence electrons can be measured in microscopic samples, thus opening the way to electron Compton experiments in polycrystalline specimens or microscopic segregates; c) Compton scattering is an extremely precise method for the investigation of otherwise undetectable solid state effects of the ground state, such as electron correlation.

Acknowledgements

This work was sponsored by the Austrian Fonds zur Förderung der wissenschaftlichen Forschung, project P7432-Phy.

References

[1] Bauer GE, Schneider JR. (1984). Nonlocal Exchange-Correlation Effects in the Total Compton Profile of Copper Metal. Phys. Rev. Lett. 52, 2061-2064.

[2] Bauer GW, Schneider JR. (1985). Electron correlation effect in the momentum density of copper metal. Phys. Rev. B 31, 681-692.

[3] Bloch BJ, Mendelsohn LB. (1974). Atomic L-shell Compton profiles and incohernt scattering factors: Theory. Phys. Rev. A 9, 129-154.

[4] Egerton R F. (1986). EELS in the Electron Microscope. Plenum Press, New York, 357-361.

[5] Eisenberger P, Platzman PM. (1970). Compton Scattering of X Ray from Bound Electrons. Phys. Rev. A 2, 415-423.

[6] Hansen NK, Pattison P, Schneider JR. (1987). Analysis of the 3-Dimensional Electron Distribution in Silicon Using Directional Compton Profile Measurements. Z. Phys. B Cond. Matter 66, 305-315.

[7] Pattison P, Hansen NK, Schneider JR. (1982). Anisotropy in the Compton Profile of Copper. Z.Phys. B Cond.Matter 46, 285-294.

[8] Schattschneider P, Hohenegger H. (1987). Electron Compton Scattering from Polycrystalline Aluminum. In: D. C. Joy (ed.), Analytical Electron Microscopy. San Francisco Press, 270-274.

[9] Vasudevan S, Rayment T, Williams BG. (1984). The electronic structure of graphite from Compton profile measurements. Proc. Roy. Soc. London A391, 109-124.

[10] Williams BG, Parkinson MP, Eckhardt CJ, Thomas JM. (1981). A new approach to the measurement of the momentum densities in solids using an electron microscope. Chem. Phys. Lett. 78, 434-438.

[11] Williams BG, Sparrow TG, Egerton RF. (1984). Electron Compton scattering from solids. Proc. Roy. Soc. London A393, 409-422.

[12] Williams BG, Uppal MK, Brydson RD. (1987). Dynamical scattering effects in electron scattering measurements of the Compton profiles of solids. Proc. Roy. Soc. London A 409, 161-176.

Discussion with Reviewers

R. Bonham: It is well established that in regions where the Bethe surface is small, the details of the surface can be strongly influenced by channel coupling. The most serious type is coupling to the elastic channel in the case of dipole-allowed bound-bound excitations at large momentum transfer. Therefore one should be a little careful in interpreting Compton profile results obtained by electron scattering at high values of the Compton variable.

Authors: Besides multiple inelastic scattering, combined elastic-Compton scattering (i. e. coupling to the elastic channel) is in fact the main problem in electron Compton scattering. In case of a fine-crystalline specimen with randomly oriented grains the diffraction pattern is radially symmetric, and channel coupling causes a relatively smooth background, as discussed in the text. Careful background fitting should then yield reasonable results.

The case of single crystals is more complicated. Here, the excited Bragg reflections only give rise to elastic channel coupling, and the Compton profile is a superposition of cuts through the Bethe ridge at many different momentum transfers. in general, it does not have a smooth background, and fitting does not apply. An exact solution of that problem has not yet been given. However, simulation of Compton profiles relying on elastic intensities derived from dynamical diffraction theory seems to be a sound approach to the interpretation of Compton profiles, as was shown in a fundamental study by Williams and coworkers [12] .